HETG High-Order Diffraction Efficiency

K.A. Flanagan, N.S. Schulz

Center for Space Research
Massachusetts Institute of Technology
Cambridge, MA 02139

S.S. Murray

Smithsonian Astrophysical Observatory
60 Garden Street
Cambridge, MA 02138

G.D. Hartner, P. Predehl

Max-Planck-Institut fur Extraterrestrische Physik (FRG)
Garching, FRG

ABSTRACT

Measurements at XRCF produced calibration data of the high orders of the AXAF High Energy Transmission Gratings at several energies. These tests provide a necessary complement to the limited set of laboratory high-order measurements on each of the flight gratings. We present the analysis and results of these measurements made at XRCF in Phase 2, where the flight detectors, HRC and ACIS, were employed.

Keywords: X-ray, X-ray astronomy, X-ray spectroscopy, transmission grating, calibration

1. INTRODUCTION

The Advanced X-ray Astrophysics Facility (AXAF) includes two transmission grating spectrometers designed for use with the mirror assembly and with two focal plane detectors to provide high-resolution spectroscopy. The high-resolution spectrometers, the High Energy Transmission Grating (HETG) Spectrometer and the Low Energy Transmission Grating (LETG) Spectrometer, consist of individual grating elements on support structures which are inserted into the optical path behind the AXAF mirrors. In the case of the HETG, these grating elements are of two types, High Energy Gratings (HEG) and Medium Energy Gratings (MEG). The dispersed spectrum is read out by one of the two focal plane detectors: the AXAF CCD Imaging Spectrometer (ACIS), and the High Resolution Camera (HRC). In addition to its imaging capability, ACIS provides moderate spectral resolution. Details of these instruments are given elsewhere[1,2,3,4].

All of these flight components – mirrors, gratings, and detectors – were subjected to calibration testing at the X-Ray Calibration Facility (XRCF) at Marshall Space Flight Center[5]. This testing served many purposes, among them:

- compare measurements with predictions arising from calibrations at the subassembly level
- provide end-to-end testing of components brought into joint operation for the first time
- provide calibration of attributes that were unobtainable at subassembly level (i.e., testing with a subarcsecond focused beam, testing gratings under full illumination as an assembled array)
- examine unexpected behavior revealed by the unique testing configurations and conditions exercised at XRCF

An overview and detailed results of this testing program are given in companion papers at this conference[6,7,8,9,10,11].

The purpose of this paper is to examine the efficiencies of higher diffraction orders of the HETG gratings in XRCF measurements taken during Phase 2 with the ACIS and HRC instruments. Since efficiency is a property intrinsic to

the gratings, it is natural to use a technique that eliminates dependencies on the properties of the mirrors, detectors, or X-ray source. The approach taken is to determine the ratio of the higher order to the first order. The results are compared with subassembly predictions. This approach has several advantages. It is not necessary to know the incident beam flux, mirror response, or absolute detector efficiency. The beam need not be spectrally pure, since only dispersed orders are used in this analysis. However, variations in detector uniformity must be considered, as they can affect the result.

The subassembly calibration of the gratings included very few higher order measurements, and these were all done on a few isolated portions of the individual gratings. Therefore, XRCF testing was critical to calibration of the high order efficiency of the assembled grating instrument. In addition, analysis of the data has yielded insight into both the HRC-I and ACIS-S instruments in aspects that were not fully examined at subassembly level. These will be discussed further below.

2. SUBASSEMBLY EFFICIENCIES AND ERRORS

Every grating was tested for diffraction efficiency at the subassembly level. Details of the test setup[12] and calibration test analysis techniques[13] have been given in previous conferences. In subassembly testing, six energies were available: 0.93, 1.254, 1.486, 2.293, 4.511 and 6.4 keV. Among positive and negative orders, a total of 10 to 12 first order measurements and 7 or 8 second order measurements (depending on the grating) contribute to defining a best-fit set of grating bar parameters to describe each grating. The model for each grating facet is used to generate efficiencies at all AXAF energies and orders from -11 to +11. By summing these efficiencies for all the gratings and weighting them appropriately for mirror area and vignetting, the predicted efficiency for the assembled grating array is obtained. Because measured efficiencies were used to obtain the prediction, one might expect these predictions to be "reasonable" at 1st order, "fair" at 2nd order but "poor" at higher orders. Reflecting this expectation, the error bars that have been assigned nominally are 5% to 20% for 1st order efficiency (depending on energy), 20% for 2nd order, 50% at 3rd order and 90% for higher orders. The 1st order error bars and their breakdown by energy are based on synchrotron tests on a limited number of gratings, where a comparison was made between the synchrotron results and subassembly predictions. Given that the intensity of higher orders is a strong function of grating bar shape[14], the extension of the subassembly model to very high orders is tenuous, underlining the need for direct measurement at XRCF.

3. TESTS WITH HRC-I AT XRCF

HETG was tested in combination with the HRC-I in Phase 2 at XRCF. The complete series consisted of one focus check at 1.254 keV, 33 effective area tests in a defocussed configuration, and one monochromator scan with 4 energies centered on 1.54 keV. These are listed in Table 1, along with the energy and range of dispersed orders on the detector. Figure 1 shows the HRC-I with the HEG and MEG grating dispersion pattern at 7 keV. The HRC-I detector is square and the image of Figure 1 is presented in detector coordinates. The dispersion direction for the gratings is aligned approximately parallel to a diagonal of the detector, so that the number of orders detected is limited by the detector size and the intensity of the high orders. In general, the zero order position was displaced from the nominal imaging aim point in order to minimize accumulated dose in that region. Note that the direction of the bias angle of the microchannel plate is toward the top in the figure, and is not symmetric with respect to the dispersion direction. Details of the HRC-I and calibration information are given in this and prior conferences[15,16,17].

From Table 1 it is evident that HEG 2nd order is only available on the detector for energies of 1.7 keV and above. For the MEG gratings, 2nd order was suppressed and measurable at only a few energies, but third order was detectable at 1.49 keV and above. Energies below 1.254 keV were not analyzed for either grating since there were no higher orders falling on the detector. The breakdown of order by energy is given in Table 2.

3.1. Processing of the Raw Data

The HRC data were processed in several steps. The raw data files were screened for lost major frames, converted from telemetry format and degapped. Two sets of event lists were then created, with different rejection criteria based on the saturation levels of the electronics (4096 for the amplifiers and 255 for the pulse height). This approach was prompted by considering the testing conditions early in Phase 2. In the first day of the HETG + HRC-I tests, the detector high voltage was set at a relatively high level and there was a considerable number of saturated events. On succeeding days, the voltage was lowered and the relative number of saturated events decreased. Since saturation can

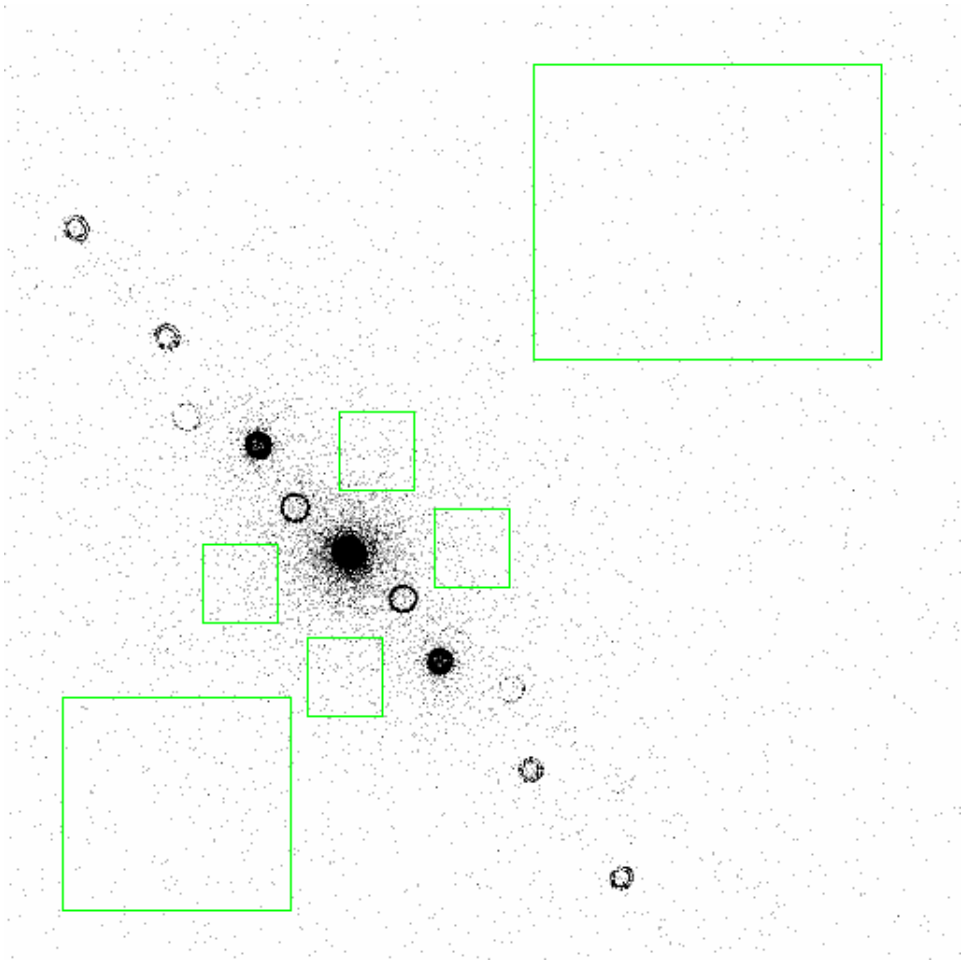

Figure 1. HETG + HRC-I test at 7 keV. Positive orders are dispersed toward the upper left in the figure. The large box, top right, is used to estimate detector background. The small boxes around zero order sample mirror-scattered events. The data have been "cleaned" to remove saturated events.

result in incorrect position assignment of the events (of order 1/2 mm or less), two separate analyses were performed on the data. In the case of "cleaned" data, all events with pulse height above 254 or with amplifier value above 4090 were rejected. In the second case, saturated events were included in the analysis (for which the data were termed "uncleaned").

A detailed investigation showed that smearing of the image due to electronic saturation did *not* systematically affect the result: ratios remained unchanged to within $\sim 3\%$ regardless of whether or not the smeared events were captured within the counting region. This is understandable since the regions of interest used were large compared to the position errors due to saturation. However, there was evidence to suggest a higher proportion of saturated events in bright orders relative to faint orders. (This is currently under study.) If so, when "cleaned" data are used, ratios formed with a bright first order are systematically enhanced (by 10% to 40%). Therefore, since saturated events represent true X-ray events and their positioning errors do not compromise the analysis, we have chosen to use the "uncleaned" data set throughout. This unusual saturation level[16] as found on the first day of these tests, was decreased on subsequent days after adjustment of the electronics and has now been eliminated in the flight instrument.

3.2. Selection of Source and Background Regions

The technique employed for selecting regions of the grating readout was to display each dataset with SAOtng (SAOimage: The Next Generation[18]). Each order of interest was captured in a simple rectangular box region, and

the number of events within each box was determined. In order to estimate the effects of background and mirror scattering, several "background" regions were selected, as illustrated in Figure 1. The largest box, distant from the zero order, is assumed to reflect approximately detector backgound. The next largest box, while distant from the zero order, nevertheless was found to have a higher ($\sim$ 2 times) background rate and is assumed to contain mirror-scattered photons. The selection of small boxes centered among zero and 1st order had a much higher ($\sim$ 8 times) background rate, which is presumed due to mirror scattering around the zero order.

In the analysis, the simple detector background was used for background subtraction for all orders. This is appropriate for the distant high orders, but there may be mirror-scattered photons captured within the first order regions. Mirror scattering is on the 1% level or less, and by using the measured "scattered rate", we found that corrections to the ratios systematically increase it by 0.5% to a few percent, a negligible effect given the counting statistics and other errors. We have neglected this correction.

3.3. Corrections and Errors

Flat field tests to measure detector spatial uniformity were not performed with the settings used on the day on which most of the HETG + HRC data were taken. However, the HRC-I was known to be *more* uniform than on subsequent days, for which uniformity data are available[16] at 4.5 keV and 1.49 keV. At 4.5 keV, the HRC-I was found to be uniform to better than 5% over the central region. At 1.49 keV, the detector QE was not as uniform as at the higher energy, but was flat at the 10% level over the central region[16] out to a radius of 30 to 35 mm. Beyond this radius the QE dropped by $\sim$ 20%. No detector uniformity corrections have been applied to the measured ratios.

It has been noted that the bias angle is not symmetric with respect to the dispersion direction. This can result in an asymmetric detection efficiency of a positive order with respect to its negative counterpart. The angle dependence of the QE is estimated to result in a difference[19] of at most a few percent, and correcting for bias angle has been neglected. In order to examine the potential effects of bias angle on the result, the ratio of the +1 order to the -1 order was taken. Any systematic asymmetry would most likely be ascribed to grating asymmetry in these orders, detector asymmetry due to bias angle, or to nonuniform QE effects across the detector (known to be small). The result is given in Figure 2 for the HEG grating, which is more likely than the MEG to show intrinsic asymmetry and which disperses across more of the HRC-I surface. The plot reflects asymmetry due to all effects: the asymmetry is obviously very small in comparison with other errors. Thus, neglect of bias angle and detector uniformity corrections is acceptable. Table 3 gives a summary of the various effects that have been discussed and their impact on the results.

3.4. HRC Results

Figure 3 shows the expected higher order ratios for the HEG and MEG gratings based on subassembly predictions. Figure 4 shows the measured HEG ratios for 2nd, 3rd and 4th orders overlaid with the prediction. (Solid points are the ratios of positive orders, hollow points refer to negative orders. The error bars reflect only counting statistics.) The 5th and 6th order ratios are similar and are not shown. The measurements appear to be systematically suppressed relative to the predictions. The approximate magnitudes of these deviations are given in Table 4 along with the typical errors due to counting statistics. Although the departures are within the errors assigned to the predictions, they exceed the counting statistics and other uncompensated correction effects, and may be deemed to be significant.

Figure 5 shows the measured MEG ratios for 2nd, 3rd, 4th and 5th orders. In general, there is fairly good agreement with the predictions. Moreover, the higher ratios (orders 6 through 9) are similar, agreeing reasonably well with the subassembly predictions. These results are summarized in Table 4.

4. ACIS TESTS AT XRCF

During Phase 2, tests of HETG with ACIS-S were performed using electron impact sources and monochromatic beams. The present analysis is limited to the those tests that employed the double crystal monochromator (DCM), which have been described in detail in a companion paper[20]. We directly incorporated the results from that study of absolute effective area to obtain the desired ratios for the present analysis.

4.1. Order Ratios

Figure 6 shows the +1 to -1 order ratio for HEG as detected by ACIS-S. The plot shows significant (up to 35%) departures from unity. As discussed previously, these may be due to intrinsic grating asymmetry or detector nonuniformity. (Bias angle considerations do not apply to the ACIS-S.) However, deviations from symmetry in Figure 2 with the HRC-I detector are less than 5%, on a par with detector uniformity. Thus, grating asymmetry cannot be expected to account for the structure seen in Figure 6. These arise from variations within the detector. The jumps seen at 1.7 keV and 2.9 keV coincide with points at which one of the orders traverses a boundary between a frontside-illuminated (FI) and a backside-illuminated (BI) device. Between these energies, the +1 and -1 orders are both captured on FI chips, but outside that range the one order falls on a BI chip, the other falls on a FI chip. It is clear that this strong residual structure, due to the detector, will complicate interpretation of the higher order ratios. It is worth remembering that in the analysis[20], the quantum efficiency functions were not yet avaliable for each device and templates were used for each CCD type. Thus, chip-to-chip discontinuities would be expected at this level of analysis.

Figure 7 shows the HEG 2nd, 3rd, 4th and 5th order ratios. Ratios between positive orders are denoted with filled boxes, whereas those between negative orders are marked by hollow boxes. In each one of these plots, there is a strong enhancement above 7 keV. Since it is common to all four order ratios, it likely arises from a supression of first order effective area. From the 2nd order ratio, it is clear that this feature is far stronger it the -2/-1 ratio (where the -1 order is captured by a FI device) than in the +2/+1 ratio (where the +1 order lands on the S3 chip, a BI device). The 3/1 ratio agrees generally with the HRC-I results over the energy range of 3 to 5 keV, but then the ratio is enhanced above 5 keV and shows other structure. In general, the HEG ratios with ACIS-S show much structure and do not reproduce the systematic reduction relative to predictions as shown with the HRC-I.

Figure 8 shows the MEG 3rd, 5th, 7th and 9th order ratios. The 3rd and 5th orders show enhancements above 5 keV, but there appear to be some smooth regions (2.5 to 4.5 keV) which agree reasonably well with predictions.

The features that have been noted can be traced to detector effects (grade migration, charge loss and "blooming") which will be discussed below.

4.2. Discussion of ACIS results

The effective areas presented by Schulz et al.[20] show that in general the measurements agree with the expected effective area function to quite a high degree. However, there are significant local deficiencies that remain. The most prominent (see Figure 11 of Schulz et al.[20]) is an apparent drop of effective area for HEG +1 and -1 orders below the expectation at energies above 5 keV.

One possible explanation given in that paper was a local non-uniformity effect in the beam to which the HEG, because of its smaller aperture, would be more susceptible than the MEG. (In the MEG such a drop is not significantly visible in the data.) However, the observed drop in HEG area sometimes exceeds 10%, which would need a quite strong local non-unifomity in the beam. This is unlikely since the DCM beam at higher energies has been measured to be very uniform overall. In addition, if beam nonuniformities were the cause, the 2nd order effective area would also show this deficiency, but it does not.

A more plausible explanation, which we are currently investigating, are deficiencies in the CCD quantum efficiencies caused by grade migration and lost charge effects at high energies and high fluences (cts/s/cm^2). This has been described in detail by Allen et al.[7] Similar corrections were used by Schulz in order to correct deficiencies observed in the zero order effective area. The effects are triggered by the higher fluence at XRCF, which causes events to overlap more often and forces a migration into higher number grades in the event detection algorithm. At even higher energies, charge cloud overlaps may prevent the detection of the event. Again, the HEG is more susceptible to these effects since the fluence in the HEG image at XRCF is generally higher than in the MEG image (recall that the HEG mirror shells are of smaller diameter). Although the first order areas presented in Schulz show clear fingerprints of these effects at work, the uncertainty of the beam uniformity issue remains unresolved.

A comparison of the higher orders to the first order has an advantage over the effective area analysis in that beam uniformity issues are removed – only effects caused by the science instruments are left. Since a quantitative evaluation is still in progress, we restrict ourselves for now to a merely qualitative description of effects and emphasize that the following interpretations should be treated with caution.

During subassembly testing of the ACIS instrument, fluences were low and grade migration and lost charge effects were not observed[21]. Although the focused beam at XRCF increases the fluence, the higher order grating efficiencies are low enough that fluences in these orders drop below those of subassembly testing. Thus, grade migration and lost charge effects should not be noticed in any order other than 1st. Key indicators for grade migration and charge loss effects are the ratios of the lower orders to the first orders. (Higher order ratios will have poor counting statistics and large uncertainties.) Figures 7a and 8a show the HEG 2nd to 1st order ratio and the MEG 3rd to 1st order ratio. The solid line indicates the prediction. Clearly, in both figures the ratios start to deviate from the prediction above 5 keV, suggesting a deficiency in the 1st order effective area. Here the HEG, as expected, shows the strongest deviations. Above 5 keV we probably see the effects of grade migration, and above 7 keV the additional effect of charge loss. The latter effect is more pronounced in the negative order ratio (empty squares) where the 1st order appears on a FI device, as compared to the positive ratio (filled squares), where the 1st order appears on a BI device. This is consistent with the related effect of 'blooming' caused by high energy events in FI devices; it is not seen in BI devices[22,23]. The effects are also observed in the HEG 3rd and MEG 5th order ratios. At higher orders, the ratios follow the predictions nicely, however the data show significant scatter due to poor counting statistics.

We can rule out the possibility that these effects are caused by the grating itself, because they are not observed in analogous measurements with the HRC-I. As discussed earlier, the near-perfect symmetry of the +1 and -1 orders (to within 5%) of the HEG with HRC-I exclude the grating as a contributor to these effects.

5. CONCLUSIONS

We have examined the ratios of higher grating orders with respect to the first order for Phase 2 tests of HETG with the flight instruments, HRC-I and ACIS-S. We found that:

- The symmetry of the +1 and -1 orders of HEG with HRC-I lead to the conclusion that detector nonuniformity, grating asymmetry and bias angle effects were small.
- HRC measurements show suppressed higher grating orders for HEG relative to predictions. Measurements of the MEG orders agree well with predictions.
- ACIS-S shows strong detector effects, compatible with grade migration and charge loss.
- Subassembly fluences were too low to trigger charge migration and charge loss effects in ACIS. These calibration tests, and the ratio technique we have employed, have provided useful means for probing these detector effects.

Several items remain for future work. These include:

- Investigate the relation between saturation and count rate density in HRC-I.
- Quantitative analysis of grade migration and charge loss in ACIS.
- Incorporate synchrotron high order measurements.
- Examine Phase 1 measurements for high orders and asymmetry.
- Analyze EIPS sources with both detectors and the monochromator scan with HRC-I.

6. ACKNOWLEDGMENTS

We thank D. Dewey and H. Marshall for helpful discussions. We are grateful to Andrea Prestwich for assistance with data reduction techniques. We are indebted to Eric Mandel for providing assistance with an updated version of SAOtng for use in this analysis. We thank Eric Fischbach for assistance with manuscript preparation. This work was prepared under NASA contracts NAS8–38249 and NAS8–39073.

7. REFERENCES

1. T.H. Markert, C.R. Canizares, D. Dewey, M. McGuirk, C. Pak, M.L. Schattenburg, *SPIE Proceedings* **2280**, 168 (1994).

2. M.V. Zombeck, J.H. Chappell, A. Kenter, R.W. Moore, S.S. Murray, *SPIE Proceedings* **2518**, 96 (1996).

3. P. Predehl, H. Kraus, H.W. Bruninger, W. Burkert, G. Kettenrin, H. Lochbihler, *SPIE Proceedings* **1743**, 476 (1992).

4. D.H. Lumb, M.W. Bautz, D.N. Burrows, J.P. Doty, G.P. Garmire, P. Gray, J.A. Nousek, G.R. Ricker, *SPIE Proceedings* **2006**, 265 (1993).

5. M.C. Weisskopf and S.L. O'Dell, *SPIE Proceedings* **3113**, 2 (1997).

6. M.C. Weisskopf and S.L. O'Dell, *SPIE Proceedings* **3444**, (1998).

7. C.L. Allen, P.P. Plucinsky, B.R. McNamara, R.J. Edgar, N.S. Schulz, J.W. Woo, *SPIE Proceedings* **3444**, (1998).

8. M.W. Bautz, F. Baganoff, T. Isobe, S.E. Jones, S.E. Kissel, B. LaMarr, H.L. Manning, M. Pivovaroff, G.Y. Prigozhin, J.A. Nousek, C.E. Grant, K. Nishikida, F. Scholze, R. Thornagel, G. Ulm, *SPIE Proceedings* **3444**, (1988).

9. J.E. Davis, H.L. Marshall, M.L. Schattenburg, D. Dewey, *SPIE Proceedings* **3444**, (1988).

10. M.D. Stage and D. Dewey, *SPIE Proceedings* **3444**, (1998).

11. D.A. Swartz, R.F. Elsner, J.J. Kolodziejczak, S.L. O'Dell, A.F. Tennant, M.E. Sulkanen, M.C. Weisskopf, R.J. Edgar, *SPIE Proceedings* **3444**, (1998).

12. D. Dewey, D.N. Humphries, G.Y. McLean, D.A. Moschella, *SPIE Proceedings* **2280**, 257 (1994).

13. K.A. Flanagan, D. Dewey, L. Bordzol, *SPIE Proceedings* **2518**, 438 (1995).

14. T.H. Markert, D. Dewey, J.E. Davis, K.A. Flanagan, D.E. Graessle, J.M. Bauer, C.S. Nelson, *SPIE Proceedings* **2518**, 424 (1995).

15. A. Kenter, J.H. Chappell, R.P. Kraft, G.R. Meehan, S.S. Murray, M.V. Zombeck, *SPIE Proceedings* **2808**, 626 (1996).

16. S.S. Murray, J.H. Chappell, A.T. Kenter, K. Kobayashi, R.P. Kraft, G.R. Meehan, M.V. Zombeck, G.W. Fraser, J.F. Pearson, J.E. Lees, A.N. Brunton, S.E. Pearce, M. Barbera, A. Collura, S. Serio, *SPIE Proceedings* **3114**, 11 (1997).

17. A.T. Kenter, J.H. Chappell, K. Kobayashi, R.P. Kraft, G.R. Meehan, S.S. Murray, M.V. Zombeck, G.W. Fraser, J.F. Pearson, J.F. Lees, A.N. Brunton, S.E. Pearce, M. Barbera, A. Collura, S. Serio, *SPIE Proceedings* **3114**, 26 (1997).

18. SAOtng home page: `http://hea-www.harvard.edu/RD/ (1998).`

19. HRC Calibration web page: http://hea-www.harvard.edu/HRC/calib/hrci_qe.html (1998).

20. N.S. Schulz, D. Dewey, H.L. Marshall, *SPIE Proceedings* **3444**, (1998).

21. M. Bautz, J. Nousek, G. Garmire and the ACIS instrument team, "Science Instrument Calibration Report for the AXAF CCD Imaging Spectrometer (ACIS)", available at http://wwwastro.msfc.nasa.gov/xray/axafps.html (1997).

22. AXAF Science Center, "AXAF Proposers Guide", Rev. 1.0, available at http://asc.harvard.edu (1997).

23. P. Plucinsky, private communication.

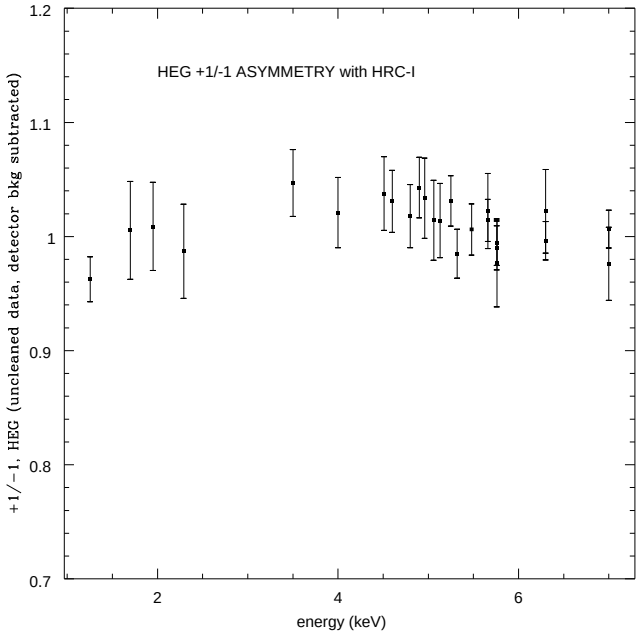

Figure 2. Ratio of +1 to -1 for HEG grating on HRC-I. In general, departures from unity are expected to be caused by intrinsic grating asymmetry, detector nonuniformity or bias angle effects.

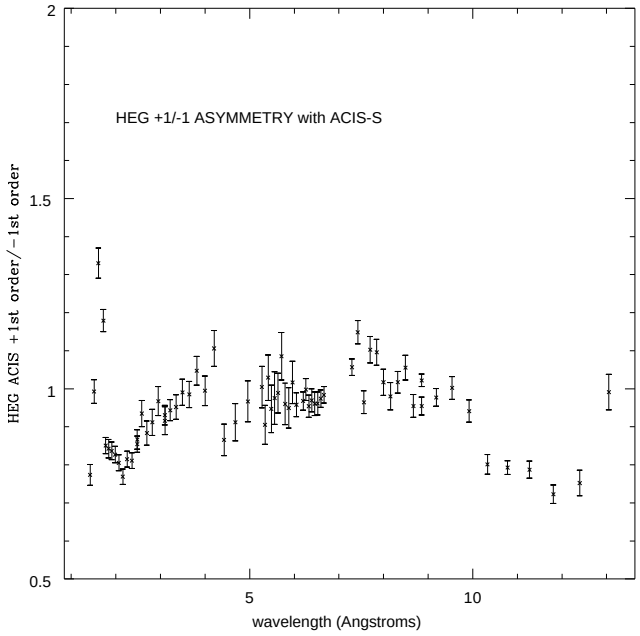

Figure 6. Ratio of +1 to -1 for HEG grating on ACIS-S. Structure is due to detector effects.

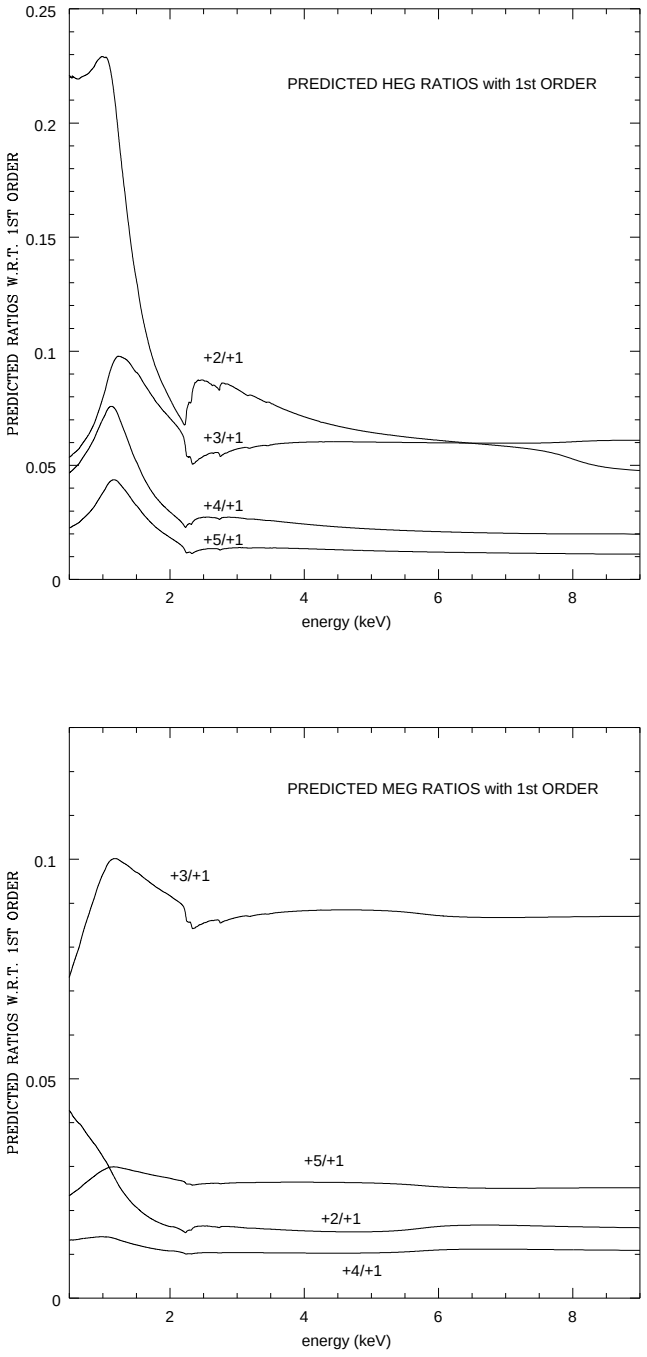

Figure 3. Expected ratios of orders 2 through 5 with respect to 1st order for HEG (top) and MEG (bottom). These are based on subassembly calibrations.

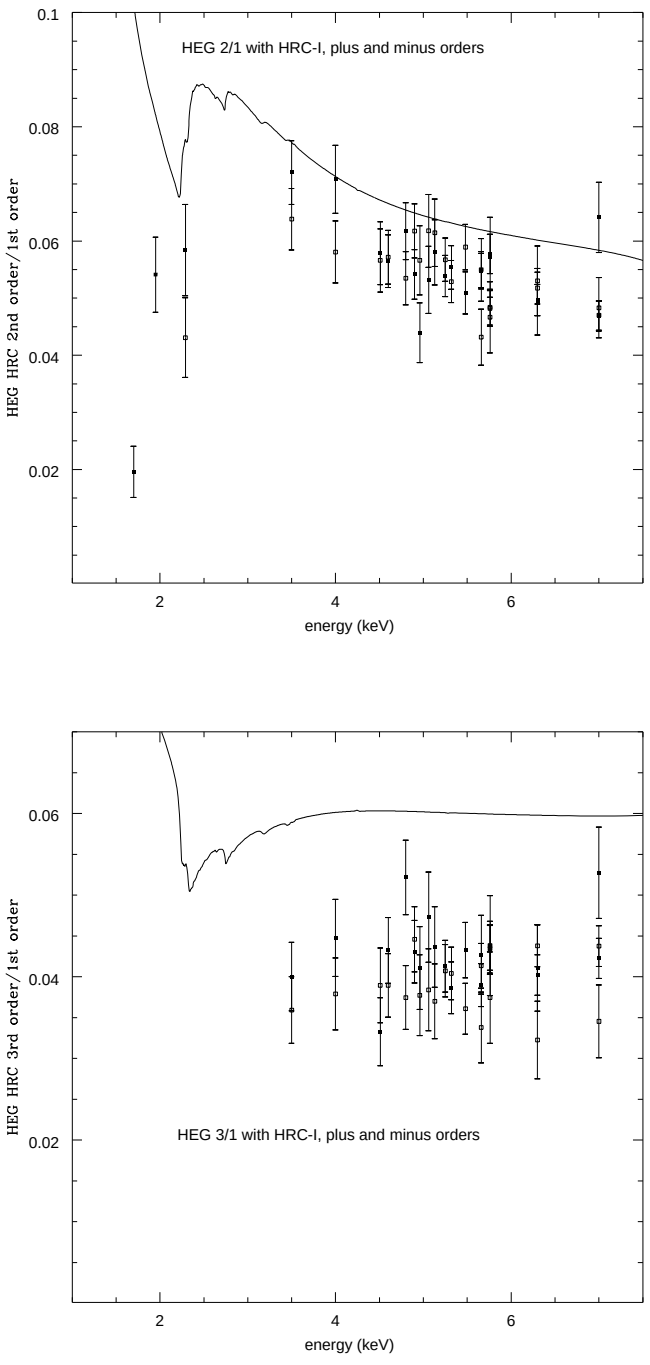

Figure 4. Measured HEG ratios for 2nd,3rd, and 4th orders with HRC-I. The solid curve represents the predicted ratios. Hollow points indicate ratios of negative orders, and solid points refer to positive orders. The error bars are due to counting statistics. The measurements systematically fall below predictions.

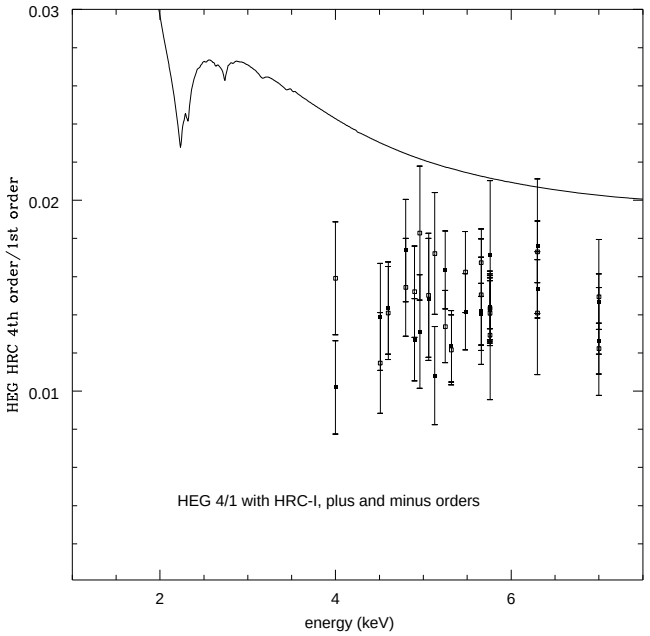
0.03
0.02
0.01
HEG HRC 4th order/1st order
HEG 4/1 with HRC-I, plus and minus orders
2
4
6
energy (keV)

Run ID	TRW ID	Energy	HEG orders	MEG Orders	Comments
i0810621	G-HHI-EA-7.048	7.0	+6 to-6	+3 to -5	
i0811327	G-HHI-EA-99.059	7.0	+4 to -4	+3 to -5	
i0810657	G-HHI-EA-7.047	6.3	+6 to -5	+8 to -5	
i0811342	G-HHI-EA-99.060	6.3	+4 to -4	+8 to -3	
i0810725	G-HHI-EA-7.046	5.76	+5 to -5	+8 to -5	
i0811356	G-HHI-EA-99.061	5.76	+4 to -4	+5 to -5	
i0810804	G-HHI-EA-7.045-1	5.66	+5 to -5	+8 to -9	
i0810756	G-HHI-EA-7.045	5.66	+5 to -5	+5 to -7	
i0810831	G-HHI-EA-7.044	5.48	+5 to -4	+7 to -5	
i0810855	G-HHI-EA-7.043	5.32	+5 to -4	+7 to -8	
i0810916	G-HHI-EA-7.042	5.25	+5 to -4	+8 to -7	
i0810936	G-HHI-EA-7.041	5.13	+4 to -4	+5 to -5	
i0810950	G-HHI-EA-7.040	5.05999	+4 to -4	+6 to -5	
i0811005	G-HHI-EA-7.039	4.96	+4 to -4	+5 to -7	
i0811019	G-HHI-EA-7.038	4.9	+4 to -4	+7 to -8	
i0811037	G-HHI-EA-7.037	4.8	+4 to -4	+7 to -5	
i0811054	G-HHI-EA-7.036	4.59999	+4 to -4	+7 to -5	
i0811114	G-HHI-EA-7.035	4.51	+4 to -4	+7 to -5	
i0811132	G-HHI-EA-7.034	4.0	+4 to -4	+7 to -7	
i0811155	G-HHI-EA-7.033	3.5	+3 to -3	+7 to -6	MEG 2 overlaps HEG 1. Not corrected.
i0811238	G-HHI-EA-7.032	2.29	+2 to -2	+4 to -4	
i0811414	G-HHI-EA-7.031	1.95	+2 to -1	+4 to -4	
i0811434	G-HHI-EA-7.030	1.7	+2 to -1	+3 to -3	
i0940311	G-HHI-EA-9.018	1.48693		+3 to -3	MEG only. Has contaminant line..
i0911019	G-HHI-EA-6.002	1.254		+2 to -2	MEG only. EIPS - broad line.
i0911034	G-HHI-EA-6.003	1.254	+1 to -1		HEG only. EIPS - broad line.
i0910739	G-HHI-FC-1.003-Q1	1.254	+1 to -1	+2 to -2	
i0910817	G-HHI-FC-1.003-Q2	1.254	+1 to -1	+2 to -2	
i0910854	G-HHI-FC-1.003-Q3	1.254	+1 to -1	+2 to -2	
i0910931	G-HHI-FC-1.003-Q4	1.254	+1 to -1	+2 to -2	
i0940337	G-HHI-9.019	1.17595		+1 to -1	MEG only. W contaminant line.
i0811452	G-HHI-10.003	1.54	+1 to -1	+3 to -2	Energy scan; analysis pending.
i0940357	G-HHI-9.020	0.95996			Not analyzed
i0902304	G-HHI-6.004	0.9297			Not analyzed. MEG only.
i0902318	G-HHI-6.006	0.9297			Not analyzed. HEG only.
i0940427	G-HHI-9.021	0.75996			Not analyzed
i0901229	G-HHI-6.005	0.705			Not analyzed
i0940505	G-HHI-9.022	0.70499			Not analyzed
i0900251	G-HHI-6.001	0.5249			Not analyzed. MEG only.
i0900336	G-HHI-6.001-b	0.5249			Not analyzed. MEG only. Contains O.

Table 1. Summary of HETG + HRC-I higher order data.

Order	HEG Energy range	MEG Energy range	Comments
2	1.7 to 7.0	1.254, 1.7, 1.95, 2.29	not sufficiently detectable at other energies
3	3.5 to 7.0	1.48693 to 7.0	
4	4.0 to 7.0	1.95 to 6.3	not sufficiently detectable at 7.0
5	5.25 to 7.0	3.5 to 7.0	
6	6.3 and 7.0 only	3.5 to 6.3 except 5.13	
7		3.5 to 5.76 except 5.05999, 5.13	
8		4.9, 5.25, 5.32, 5.66, 5.76, 6.3	
9		5.66 only	

Table 2. Energy ranges of the measured HETG + HRC-I higher orders.

Error	magnitude	Comments
Counting Statistics	10% to 30% (see Table 4)	accounted for in analysis
Background subtraction	up to 3%, systematic	only detector background used
bias angle	few percent	neglected
detector QE nonuniformity	5 to 10% within 35 mm radius; edges drop by 20%	neglected
Event saturation	10 % to 40% systematic	accounted for: all events included

Table 3. Corrections, Systematic Effects and Errors for HETG + HRC-I

Grating	order ratio	Typical counting statistics	Assigned Subassy error	deviation from predicted
HEG	2/1	10%	20 to 25%	-10 to -15%
	3/1	10%	50%	-35%
	4/1	15%	90%	-35%
	5/1	20%	90%	-60%
	6/1	20%	90%	-60%
MEG	2/1	15%	20 to 25%	approximately correct
	3/1	10%	50%	-5%
	4/1	20%	90%	+25%
	5/1	20%	90%	-25%
	6/1	20%	90%	approximately correct
	7/1	20%	90%	-25%
	8/1	30%	90%	approximately correct
	9/1	30%	90%	-45%

Table 4. Comparison of Predictions with Measured ratios for HETG + HRC-I higher orders.

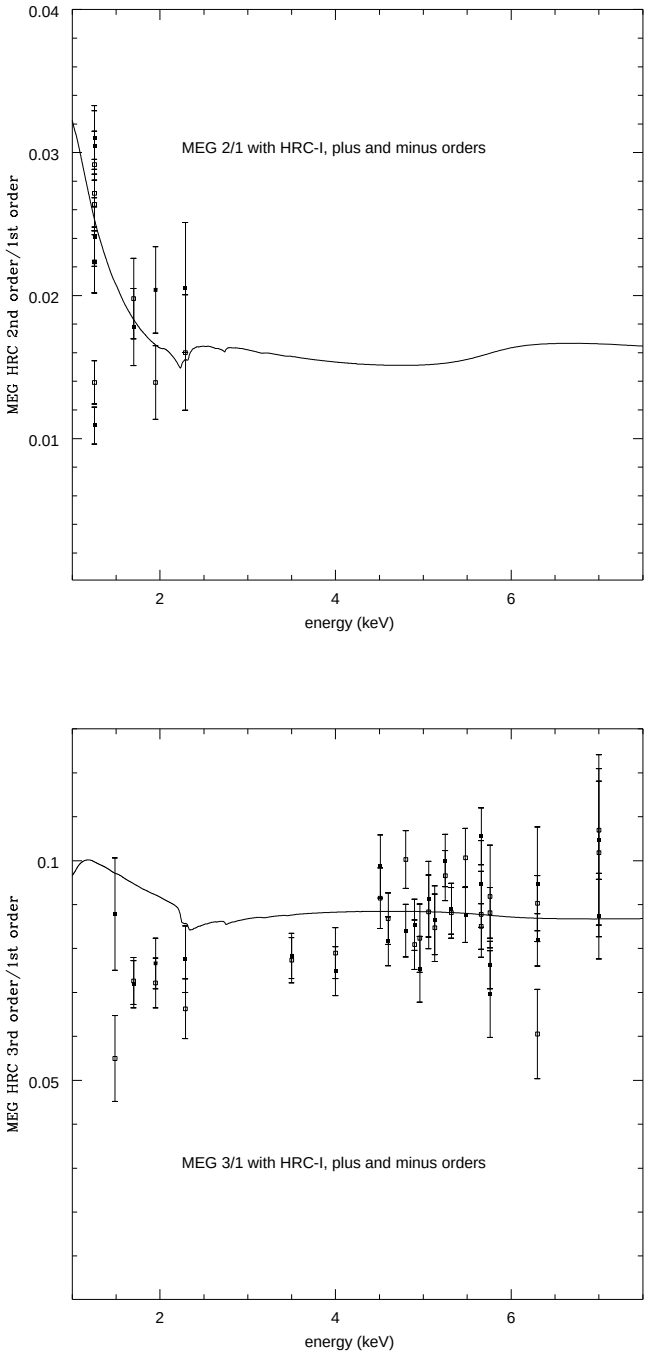

Figure 5. Measured MEG ratios for 2nd,3rd, 4th and 5th orders with HRC-I. The measured values agree fairly well with the predictions.

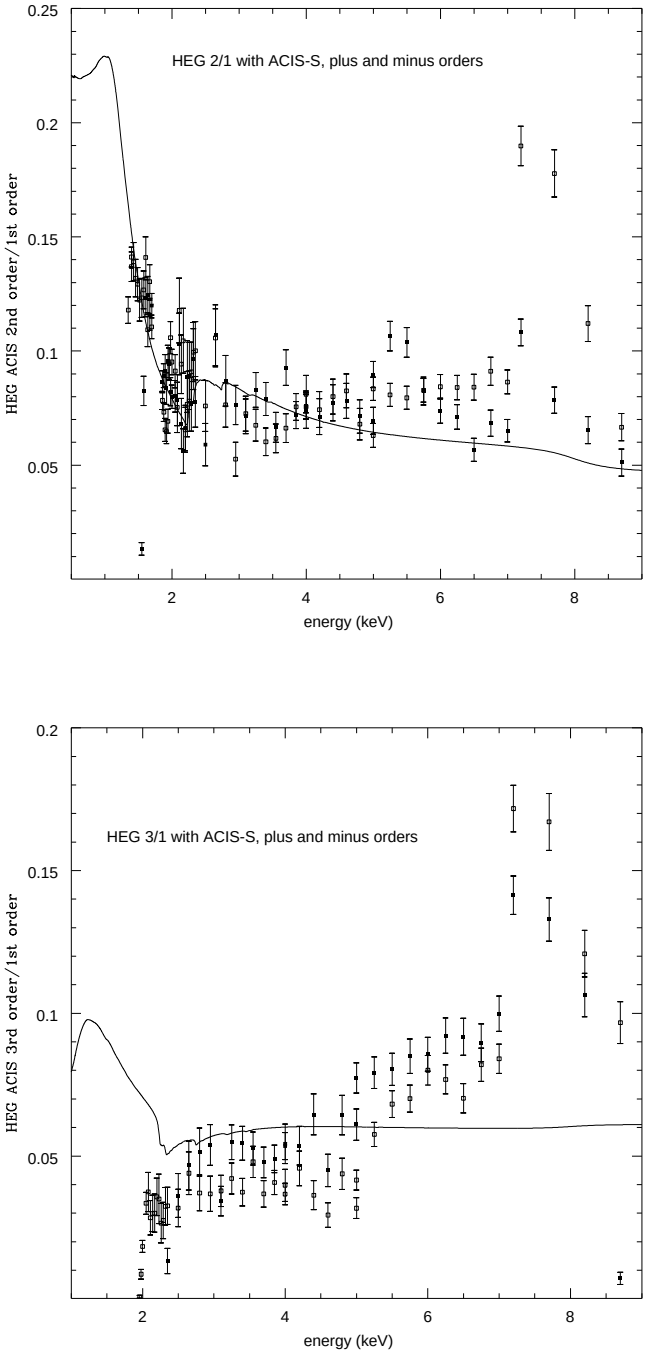

Figure 7. Measured HEG ratios for 2nd, 3rd, 4th and 5th orders with ACIS-S.

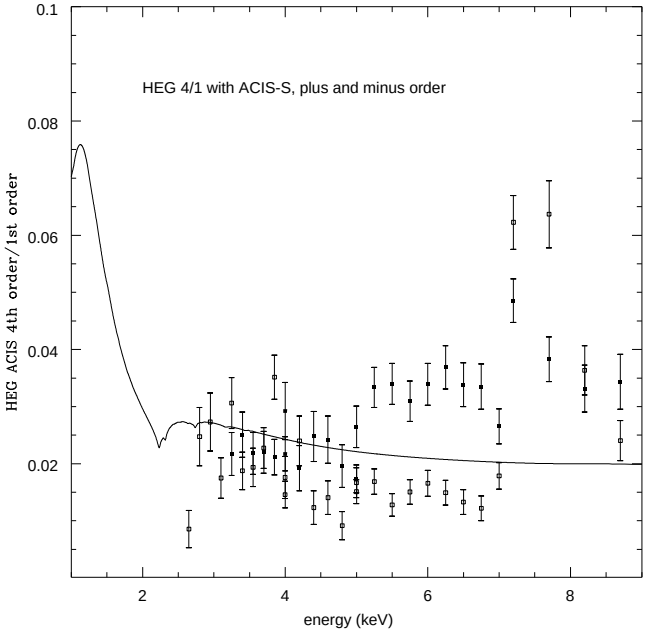
HEG 4/1 with ACIS-S, plus and minus order
HEG ACIS 4th order/1st order
energy (keV)
0.1
0.08
0.06
0.04
0.02
2
4
6
8

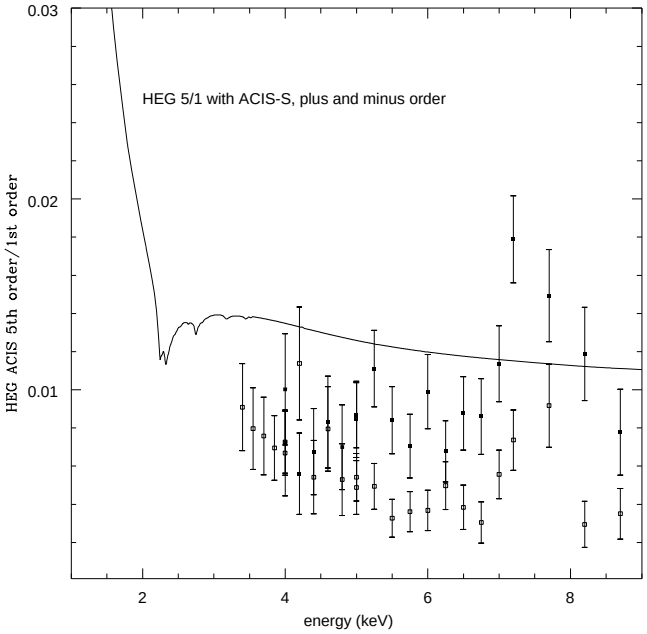
HEG 5/1 with ACIS-S, plus and minus order
HEG ACIS 5th order/1st order
energy (keV)
0.03
0.02
0.01
2
4
6
8

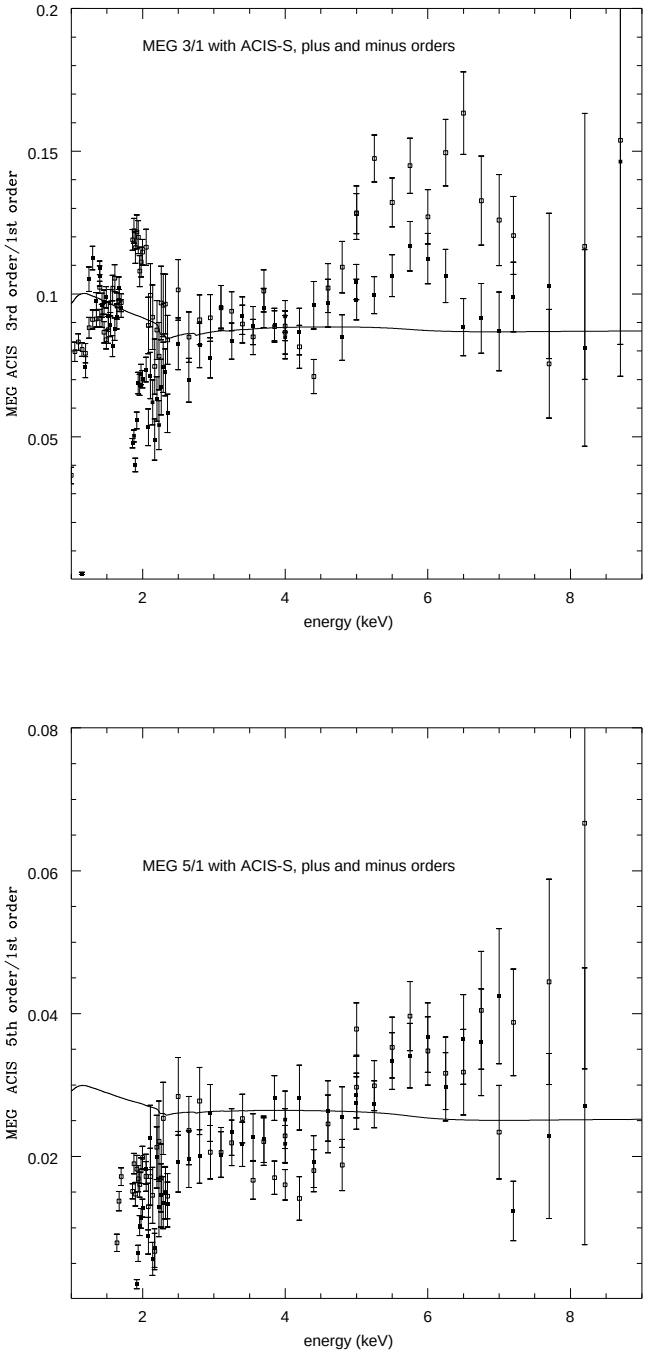

Figure 8. Measured MEG ratios for 3rd, 5th and 7th and 9th orders with ACIS-S.

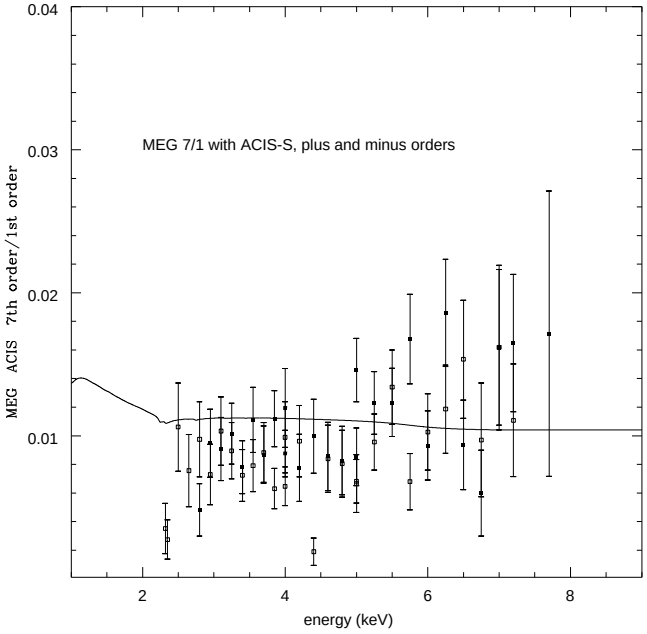
MEG 7/1 with ACIS-S, plus and minus orders
MEG ACIS 7th order/1st order
0.04
0.03
0.02
0.01
2
4
6
8
energy (keV)

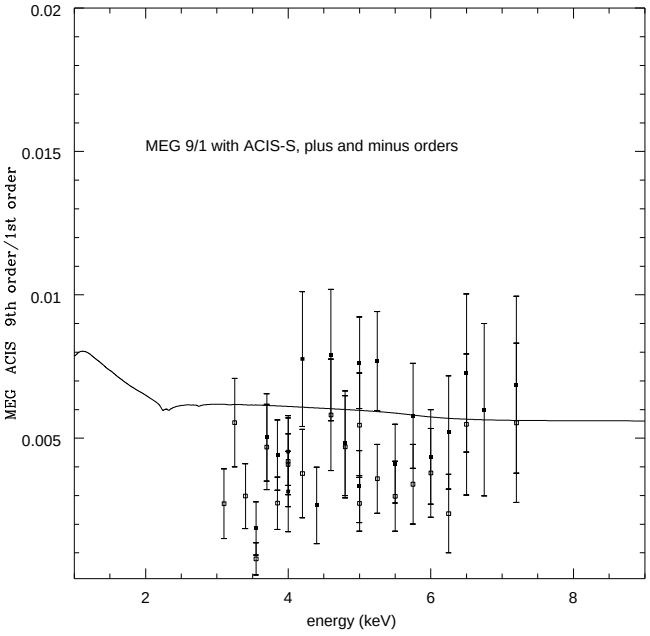
MEG 9/1 with ACIS-S, plus and minus orders
MEG ACIS 9th order/1st order
0.02
0.015
0.01
0.005
2
4
6
8
energy (keV)